Formaldehyde production from isoprene oxidation across NO_x regimes

G. M. Wolfe[1,2], J. Kaiser[3], T. F. Hanisco[2], F. N. Keutsch[4], J. A. de Gouw[5,6], J. B. Gilman[5,6], M. Graus[5,6,a], C. D. Hatch[7], J. Holloway[5,6], L. W. Horowitz[8], B. H. Lee[9], B. M. Lerner[5,6], F. Lopez-Hilifiker[9,b], J. Mao[8,11], M. R. Marvin[10], J. Peischl[5,6], I. B. Pollack[5,6], J. M. Roberts[6], T. B. Ryerson[6], J. A. Thornton[9], P. R. Veres[5,6], C. Warneke[5,6]

[1]Joint Center for Earth Systems Technology, University of Maryland Baltimore County, Baltimore, MD, USA

[2]Atmospheric Chemistry and Dynamics Laboratory, NASA Goddard Space Flight Center, Greenbelt, MD, USA

[3]Department of Chemistry, University of Wisconsin-Madison, Madison, WI, USA

[4]School of Engineering and Applied Sciences and Department of Chemistry and Chemical Biology, Harvard University, Cambridge, MA, USA

[5]Cooperative Institute for Research in Environmental Sciences, University of Colorado Boulder, Boulder, CO, USA

[6]Chemical Sciences Division, NOAA Earth System Research Laboratory, Boulder, CO, USA

[7]Department of Chemistry, Hendrix College, Conway, AR, USA

[8]NOAA Geophysical Fluid Dynamics Laboratory, Princeton, NJ, USA

[9]Department of Atmospheric Sciences, University of Washington, Seattle, WA, USA

[10]Department of Chemistry, University of Maryland, College Park, MD, USA

[11]Program in Atmospheric and Oceanic Sciences, Princeton University, Princeton, NJ

[a]Now at Institute of Atmospheric and Cryospheric Sciences, Innsbruck University, Austria

[b]Now at Laboratory of Atmospheric Chemistry, Paul Scherrer Institut, 5232 Villigen, Switzerland

Correspondence to G. M. Wolfe (glenn.m.wolfe@nasa.gov)

Abstract

The chemical link between isoprene and formaldehyde (HCHO) is a strong, non-linear function of NO_x (= NO + NO_2). This relationship is a linchpin for top-down isoprene emission inventory verification from orbital HCHO column observations. It is also a benchmark for overall photochemical mechanism performance with regard to VOC oxidation. Using a comprehensive suite of airborne *in situ* observations over the Southeast U.S., we quantify HCHO production across the urban-rural spectrum. Analysis of isoprene and its major first-generation oxidation products allows us to define both a "prompt" yield of HCHO (molecules of HCHO produced per molecule of freshly-emitted isoprene) and the background HCHO mixing ratio (from oxidation of longer-lived hydrocarbons). Over the range of observed NO_x values (roughly 0.1 – 2 ppbv), the prompt yield increases by a factor of 3 (from 0.3 to 0.9 ppbv $ppbv^{-1}$), while background HCHO increases by a factor of 2 (from 1.6 to 3.3 ppbv). We apply the same method to evaluate the performance of both a global chemical transport model (AM3) and a measurement-constrained 0-D steady state box model. Both models reproduce the NO_x dependence of the prompt HCHO yield, illustrating that models with updated isoprene oxidation mechanisms can adequately capture the link between HCHO and recent isoprene emissions. On the other hand, both models under-estimate background HCHO mixing ratios, suggesting missing HCHO precursors, inadequate representation of later-generation isoprene degradation and/or under-estimated hydroxyl radical concentrations. Detailed process rates from the box model simulation demonstrate a 3-fold increase in HCHO production across the range of observed NO_x values, driven by a 100% increase in OH and a 40% increase in branching of organic peroxy radical reactions to produce HCHO.

1 Introduction

Formaldehyde (HCHO) is a ubiquitous byproduct of volatile organic compound (VOC) oxidation. While methane is the principal HCHO precursor in remote regions, larger VOC are the main source over continents. HCHO is also directly emitted via biomass burning (Lee et al., 1997), fossil fuel combustion (Luecken et al., 2012), natural gas flaring (Knighton et al., 2012), ethanol refining (de Gouw et al., 2015), possibly vegetation (DiGangi et al., 2011) and agricultural activity (Kaiser et al., 2015a), but chemical production dominates the global budget (Fortems-Cheiney et al., 2012). Photolysis and reaction with OH destroy HCHO with

a characteristic lifetime of several hours during midday, implying that the HCHO abundance reflects recent VOC oxidation.

Globally, isoprene is the main precursor of near-surface HCHO. A highly reactive diene emitted by vegetation, isoprene comprises roughly one third of all non-methane VOC emissions (Guenther et al., 2012). Oxidation of isoprene in the presence of nitrogen oxides (NO_x = NO + NO_2) stimulates the production of ozone (Trainer et al., 1987) and organic aerosol precursors (Xu et al., 2015), impacting air quality and climate in many continental regions. Biogenic emission inventories struggle to accurately represent the spatiotemporal variability of isoprene emissions, with model-measurement discrepancies and differences among emission inventories approaching a factor of 2 or more (Carlton and Baker, 2011; Warneke et al., 2010). Such differences directly impact predicted ozone and aerosol distributions (Hogrefe et al., 2011).

Numerous studies have applied satellite-based HCHO column observations as a top-down constraint on isoprene emissions (see Kefauver et al. (2014) for a review). Typically, a chemical transport model is employed both to supply *a priori* HCHO vertical distributions for satellite retrievals (González Abad et al., 2015) and to relate HCHO column concentrations to isoprene emission strength. Early studies utilized linear steady-state relationships (Palmer et al., 2003), while recent computational advances have permitted full inversions that more fully account for transport, multiple sources and varying chemical regimes (Fortems-Cheiney et al., 2012). Such techniques have informed isoprene emission inventories in North America (Abbot et al., 2003; Millet et al., 2008; Millet et al., 2006; Palmer et al., 2006; Palmer et al., 2003), South America (Barkley et al., 2013; Barkley et al., 2008), Europe (Curci et al., 2010; Dufour et al., 2009), Africa (Marais et al., 2012), Asia (Fu et al., 2007; Stavrakou et al., 2014), and globally (Fortems-Cheiney et al., 2012; Shim et al., 2005; Stavrakou et al., 2009). Future geostationary observations, such as the NASA Tropospheric Emissions: Monitoring of Pollution (TEMPO, http://science.nasa.gov/missions/tempo/) mission, will permit an even more detailed investigation of the spatial and temporal variability of isoprene emissions and other VOC sources.

Chemistry dictates the relationship between HCHO columns and underlying isoprene emissions. Many of the above-listed studies apply 0-D box model calculations to evaluate the yield of HCHO from isoprene as a function of oxidation time, NO_x regime and chemical mechanism. In all cases, it is found that NO_x enhances both the production rate and ultimate

yield of HCHO. Slower production at lower NO_x can lead to "smearing," whereby HCHO production is displaced relative to the isoprene source. Palmer et al. (2003) define a characteristic smearing length scale, which can range from 10 to 100 km or more. Furthermore, accumulation of oxygenated VOC over multiple generations of isoprene degradation can contribute to substantial background HCHO production, which is not directly linked with fresh isoprene emissions. Long-lived primary anthropogenic or biogenic emissions, like methane and methanol, can also contribute to this background. Background column concentrations are typically on the order of 5×10^{15} cm^{-2}, equal to 20% or more of the isoprene-driven HCHO column enhancement (Barkley et al., 2013; Millet et al., 2006). A wave of recent theoretical (Peeters et al., 2014; Peeters and Müller, 2010; Peeters et al., 1999), laboratory (Crounse et al., 2012; Crounse et al., 2011; Paulot et al., 2009a; Paulot et al., 2009b) and field (Mao et al., 2012) research has highlighted shortcomings in low-NO_x isoprene oxidation schemes. Such issues translate directly into top-down emission estimates; for example, Marais et al. (2012) report an uncertainty of 40% in satellite-derived African isoprene emissions at high-NO_x and 40-90% at low-NO_x. Coarse resolution of averaged satellite observations and model simulations (typically 1° × 1° or more) has partly mitigated these problems in prior work, as variability in NO_x-dependent smearing and background production is averaged out. A more careful treatment will be needed to harness the enhanced resolution of near-future orbital observations (e.g., 8×4.5 km^2 for TEMPO), especially since these measurements will include diurnal variability.

Here, we use a comprehensive set of *in situ* observations to quantify the impact of NO_x on the isoprene-HCHO chemical link. Using isoprene and its unique first-generation products, we segregate HCHO into two categories. The first, defined as "prompt" HCHO, is produced from fresh isoprene emissions (on a timescale of less than a day) and retains the signature of isoprene emission source strength. The second category is "background" HCHO stemming from oxidation of longer-lived isoprene oxidation products and other VOC. We examine the NO_x dependence of both quantities. Applying the same method to 0-D and global model simulations, we evaluate the ability of current chemical mechanisms to replicate the observed trends. Box model results are also used to elucidate the mechanistic underpinnings of the NO_x influence on HCHO production.

2 SENEX Observations

The Southeast Nexus (SENEX) mission was an airborne campaign designed to examine the interaction of natural and anthropogenic emissions (Warneke et al., 2016). During June and July of 2013, the NOAA WP-3D aircraft logged about 120 flight hours over 20 research flights in a range of environments throughout the Southeast United States, including urban centers, power plant plumes, natural gas extraction regions, agricultural areas and forests. The payload included a suite of gas- and particle-phase instrumentation. Here we utilize observations of HCHO, isoprene, methyl vinyl ketone (MVK), methacrolein (MACR), NO and NO_2. HCHO was measured at 1 Hz by the NASA In Situ Airborne Formaldehyde (ISAF) instrument, which utilizes the laser-induced fluorescence technique and has an accuracy of ±10% (Cazorla et al., 2015). Isoprene, MVK and MACR were measured by both a quadrupole proton transfer reaction mass spectrometer (PTR-MS) and the NOAA improved whole-air sampler (iWAS) with offline gas chromatography. The PTR-MS (de Gouw and Warneke, 2007) has a stated accuracy of 20% and sequentially sampled masses for isoprene (m/z +69) and the sum of MVK and MACR (m/z +71) for 1 s each with a duty cycle of 14 s. The iWAS (Lerner et al., 2016) collected 72 canister samples each flight, which were analyzed offline with gas chromatography – mass spectrometry 3-4 days post-flight. iWAS measurement uncertainty is 20% for speciated MVK and MACR and 27% for isoprene. NO and NO_2 were measured at 1 Hz via chemiluminescence coupled with a photolytic NO_2 converter (Pollack et al., 2010; Ryerson et al., 1999) with an accuracy of 5%. Data are filtered to include only daytime boundary layer conditions (solar zenith angle < 60°, radar altitude < 1 km). Influence from biomass burning (acetonitrile > 210 pptv and CO > 300 ppbv) is also removed. This procedure, along with the disjunct nature of the PTR-MS measurement, excludes 50% of all fast (1 Hz) data. After accounting for data gaps, we retain 8435 1 Hz data points and 81 iWAS samples.

Measurements of MVK and MACR may include a positive bias from conversion of isoprene hydroxyhydroperoxides (ISOPOOH) on hot metal surfaces in the sampling system (Liu et al., 2013; Rivera-Rios et al., 2014). ISOPOOH mixing ratios up to 2 ppbv were observed by the University of Washington Iodide high-resolution time-of-flight chemical ionization mass spectrometer during SENEX. Neither the NOAA PTR-MS nor the iWAS have been tested for this interference with an ISOPOOH standard, thus we cannot definitively rule out such artifacts or develop a correction factor. To our knowledge, it is not yet clear how

the putative interference depends on instrument configuration (flow rates, electric fields, etc.). Thus, caution is warranted when comparing the SENEX systems to similar, but not identical, instruments. Theoretically, this mechanism could give rise to an analogous artifact in HCHO observations. Recent laboratory tests, however, indicate that the ISOPOOH-to-HCHO conversion efficiency in ISAF is less than 5% (St. Clair et al., 2016).

We cannot unambiguously quantify the ISOPOOH artifact using observations alone, but we can gain some insight from comparing PTR-MS and iWAS data. On average, iWAS observations of MVK+MACR are ~40% higher than those from the PTR-MS (Figs. S1 and S2), suggesting a systematic bias in one or both measurements. Both instruments were calibrated using the same gas standards, and the two techniques agree well for other species such as isoprene (Lerner et al., 2016; Warneke et al., 2016), so a calibration error is unlikely. Production of oxygenated VOC in ambient air samples collected and aged in stainless steel canisters cannot be ruled out. Enhancements in MVK and MACR (above the 20% uncertainty) have been observed in canisters after aging over ~11 days (Lerner et al., 2016), though this is significantly longer than typical turn-around times for SENEX. To evaluate the potential for ISOPOOH conversion to explain this discrepancy, we plot the ratio and difference of the PTR-MS and iWAS measurements as a function of ISOPOOH in Fig. S2. While the ratio is essentially constant (iWAS/PTR-MS ~1.43), the absolute difference exhibits a strong positive correlation with ISOPOOH ($r^2 = 0.43$). The slope of this relationship implies that a conversion of 50% of ISOPOOH to MVK and/or MACR in the iWAS system would explain the difference in the two measurements. Correcting total iWAS MVK+MACR for such an artifact reduces the slope of the iWAS-PTR-MS correlation from 1.48 to 1.24 (Fig. S1B), bringing agreement to well with combined measurement uncertainties. In practice, we cannot apply such a correction to the speciated iWAS observations as the conversion efficiency may be different for each isomer. This result does not exclude the possibility of an artifact in the PTR-MS measurement, though it does suggest an upper limit ISOPOOH conversion efficiency of 50% for the PTR-MS (which would imply a conversion of 100% for the iWAS). The analysis presented in Sections 3 and 4 primarily relies on PTR-MS data due to its greater temporal coverage. Our key conclusions are not impacted by a 50% ISOPOOH correction to the PTR-MS data, thus we use the data without correction.

SENEX sampled a wide spectrum of chemical regimes (Figure 1). For the daytime boundary-layer observations presented here, maximum 1 Hz isoprene and NO mixing ratios

respectively reach 8.1 and 95 ppbv, while minima are less than a few pptv. The distributions of both isoprene and NO observations are approximately log-normal (top and right panels of Fig. 1), peaking at 1.5 ppbv and 50 pptv, respectively. Though these distributions may be biased towards areas of urban influence, the range of environments encountered during SENEX is representative of the Southeast U.S. summertime boundary layer. The long tail at the low end of the isoprene distribution is mostly associated with regions lacking significant tree cover where isoprene emissions are lower, notably Illinois and Indiana. The NO distribution spans four orders of magnitude (< 10 to ~10^4 pptv), over which radical chemistry changes markedly. At NO mixing ratios of a few hundred pptv or more, organic peroxy radicals (RO_2) react mostly with NO. At low NO (10's of pptv or less), reaction with HO_2, other RO_2 and isomerization dominate the RO_2 fate. The bulk of the NO distribution lies in a transition region for radical chemistry, making this dataset ideal for probing the anthropogenic influence on biogenic VOC oxidation.

HCHO mixing ratios (color shading in Fig. 1) range from 0.8 to 14 ppbv with a mean of 4.3 ppbv. HCHO is most abundant in regions where both isoprene and NO_x are elevated. High NO_x is often accompanied by increased concentrations of anthropogenic VOC; however, constrained box-model calculations demonstrate that isoprene is the dominant HCHO precursor even in these cases (Sect. 5). Thus, changes in radical cycling and partitioning (and not co-variance of NO_x and anthropogenic VOC) drives the observed NO_x dependence of HCHO abundance.

3 Linking Observed and Emitted Isoprene

The isoprene photochemical cascade is a multi-step process. Isoprene oxidation is initiated via reaction with the hydroxyl radical (OH), ozone, or the nitrate radical (NO_3). In the Southeast U.S., typical daytime levels for OH, ozone and NO_3 are 4×10^6 cm^{-3}, 50 ppbv and 0.1 pptv, respectively (OH and NO_3 are estimated from median box model output, see Sect. 5). The corresponding isoprene lifetimes at 298K are 0.7 h, 17 h and 160 h, respectively. Thus, reaction with OH typically constitutes 95% or more of the total daytime isoprene sink in this environment. Addition of OH and reaction with O_2 generates one of several isoprene hydroxyperoxy radicals ($ISOPO_2$). $ISOPO_2$ isomers interconvert rapidly due to reversible O_2 addition (Peeters et al., 2009) but are eventually destroyed via reaction with NO, hydroperoxy radical (HO_2), other organic peroxy radicals (RO_2) or isomerization. Most branches have the

potential to produce HCHO, with varying yields. The laboratory-derived first-generation HCHO yield from the NO pathway is ~0.6 (Atkinson and Arey, 2003), though this value may be less representative of the real atmosphere due to the very high isoprene concentrations (and very short RO_2 lifetimes) in early chamber experiments. The first-generation yield from the HO_2 pathway is ~0.06 (Liu et al., 2013). Isomerization chemistry is less well understood; the 1,5-H-shift is believed to produce HCHO with a unity yield, while the much faster 1,6-H-shift should not produce any HCHO (da Silva et al., 2010; Fuchs et al., 2013; Peeters et al., 2014; Peeters and Müller, 2010; Peeters et al., 2009). Regardless of the specific pathway, MVK or MACR are always co-produced with HCHO in the first generation. HCHO is also generated in subsequent chemistry, but on a longer timescale and from a much larger suite of precursors. For example, the OH lifetimes of MACR and MVK are respectively 3.5 and 5 times longer than that of isoprene. HCHO, MVK and MACR are also high-yield products of isoprene ozonolysis (Atkinson and Arey, 2003), but as noted above this reaction is relatively slow. Nighttime oxidation of isoprene by NO_3 radical is also likely a negligible source of these carbonyls (Brown et al., 2009). Yields are small (Atkinson and Arey, 2003; Kwok et al., 1996), and the lifetimes of MVK, MACR and HCHO are sufficiently short that any nighttime production should not influence the midday observations considered here.

Boundary layer composition reflects a mixture of emissions with various degrees of photochemical processing. To isolate the impact of "fresh" isoprene emissions, we exploit the relatively simple chemistry of MVK and MACR, which are produced via isoprene (ISOP) oxidation and lost primarily via reaction with OH.

$$\text{ISOP} + \text{OH} \rightarrow y_{MACR}\text{MACR} + y_{MVK}\text{MVK} \qquad k_1 = 2.7\times10^{-11}\, e^{390/T} \qquad \text{(R1)}$$

$$\text{MACR} + \text{OH} \rightarrow \text{products} \qquad k_2 = 8.0\times10^{-12}\, e^{380/T} \qquad \text{(R2)}$$

$$\text{MVK} + \text{OH} \rightarrow \text{products} \qquad k_3 = 2.6\times10^{-12}\, e^{610/T} \qquad \text{(R3)}$$

Rate constants (k) are taken from the IUPAC database (Atkinson et al., 2006). These reactions form the basis for a photochemical clock of isoprene oxidation (de Gouw et al., 2005; Roberts et al., 2006; Stroud et al., 2001). Integration of the kinetic equations for this system shows that the product/parent ratios are a function of the rate constants, yield (y), reaction time (t) and mean OH concentration. In the case of MACR, for example:

$$\frac{[MACR]}{[ISOP]} = \frac{y_{MACR}k_1}{k_2 - k_1}\left(1 - \exp\left((k_1 - k_2)[OH]t\right)\right) \qquad (1)$$

An analogous expression holds for MVK. As noted by Stroud et al. (2001), this "sequential reaction model" is purely chemical and does not account for the effects of mixing and transport. Indeed, this analysis relates daughter/parent ratios to an "average" photochemical age, when in fact there is a broad distribution of ages in any mixed air mass. We also implicitly assume that direct emissions (Fares et al., 2015) and deposition (Karl et al., 2010) of MVK and MACR do not significantly influence the budget of these compounds.

Two potential issues arise when applying this model to the real atmosphere. First, the yields of MVK and MACR are dependent on $ISOPO_2$ branching and are thus a non-linear function of NO_x. Previous applications of this method (de Gouw et al., 2005; Roberts et al., 2006; Stroud et al., 2001) have assumed lab-derived high-NO_x yields of 0.33 and 0.23 for MVK and MACR, respectively (Atkinson and Arey, 2003), but this may not be appropriate in the present case; furthermore, these yields are not fully consistent with current chemical mechanisms. Given the wide range of conditions sampled, we explicitly account for NO_x-dependent yields for MVK and MACR. For this purpose, we conducted a series of pseudo-chamber simulations using a box model driven by the Master Chemical Mechanism (MCM) v3.3.1 (Jenkin et al., 2015). As described in the SI, model setup mimics typical daytime conditions in the Southeast U.S. (Fig. S3B), and yields are derived using a standard procedure. Resulting yield curves (Fig. S3A) are then interpolated to observed NO mixing ratios. Second, the photochemical age (t) implied by any observed daughter/parent ratio depends on the concentration of OH, which was not measured and varies as an air mass ages. Rather than assume a single "typical" value for OH, we express photochemical age in terms of "exposure," defined here as the product of OH concentration and reaction time averaged over the photochemical lifetime of an air mass.

Figure 2 compares the observed relationship of iWAS MVK/isoprene and MACR/isoprene ratios against theoretical trends predicted by the sequential reaction model. Theoretical ratios are calculated at fixed exposures of 2, 4, 8, 12 and 16 $\times$ 10^6 OH cm^{-3} h using model derived yields for the 5^{th}/95^{th} percentiles of the observed NO distribution (NO = 20/200 pptv, y_{MVK} = 0.18/0.38, y_{MACR} = 0.11/0.20). Observed ratios of MVK/isoprene versus MACR/isoprene exhibit a tight linear correlation. Higher ratios are often associated with higher NO_x, likely reflecting enhanced OH and higher product yields in these air masses. Far downwind from isoprene and NO_x source regions, we would expect to see higher MVK/isoprene and MACR/isoprene ratios associated with lower NO_x due to removal of the

latter. The theoretical slope agrees well with observations, indicating exposures of 1 – 16 × 10^6 OH cm^{-3} h. For a typical daytime OH concentration of 4 × 10^6 cm^{-3}, this corresponds to processing times of 0.25 – 4 hours.

The assumed MVK and MACR yields dictate the correspondence between daughter/parent ratios and exposure. For example, a MACR/isoprene ratio of 1 would be consistent with an exposure of 7.9 x 10^6 OH cm^{-3} h at NO = 20 pptv versus 6.0 x 10^6 OH cm^{-3} h at NO = 200 pptv. Thus, for any given daughter/parent ratio, a higher assumed yield gives a smaller derived exposure. The ratio of y_{MVK} to y_{MACR} determines the location of the theoretical line, and the excellent agreement of this relationship with observations in Fig. 2 indicates that MCMv3.3.1 accurately represents the branching ratios for MVK and MACR production within the sampled NO_x range.

We can effectively reverse this photochemical clock to derive a proxy for the total isoprene emissions that have been released into the sample air masses (de Gouw et al., 2005). First, we calculate OH exposures from observed daughter/parent ratios by inverting Eqn. (1). To perform this calculation with PTR-MS data (which has far greater coverage than the iWAS), we partition the measured sum between MVK and MACR using MVK/MACR ratios from steady-state box model calculations (Sect. 5). Modeled MVK/MACR ratios (with an output interval of 1 minute) are linearly interpolated to the 14-second observational time base. The MVK/MACR ratio does not vary dramatically (mean ± 1σ: 2.3 ± 0.2), and using a constant ratio instead alters exposures by less than 4%. Calculated exposures range from 1 to 20 × 10^6 OH cm^{-3} h (Fig. S4A). Exposures derived from MACR are 6% lower than those from MVK on average, and we use the mean of these two values. Next, an "initial" isoprene mixing ratio, $ISOP_0$, is estimated via reverse integration of isoprene's first-order loss rate:

$$[ISOP]_0 = [ISOP]\exp(k_1[OH]t) \quad (2)$$

$ISOP_0$ represents the amount of isoprene that an air parcel would have to start with to generate the amount of isoprene, MVK and MACR observed. Thus, it is an observationally-constrained surrogate for isoprene emission strength (modulated to some degree by boundary layer height, as it is a volume-based quantity). $ISOP_0$ mixing ratios are typically 2 – 20 times higher than observed isoprene (Fig. S4B).

4 The Yield of HCHO from Isoprene

The definition of "yield" can vary with context and requires careful consideration when quantifying chemical relationships. In a mechanistic sense, the "first generation yield" refers to the amount of HCHO produced per unit isoprene consumed in the first stage of oxidation. This is analogous to the yields of MVK and MACR used in the above calculation of initial isoprene. The model-derived first-generation HCHO yield from isoprene varies by more than a factor of 2 over the range of chemical environments encountered during SENEX (Fig. S3). An alternative definition is that of the "total yield" (sometimes referred to as the "molar yield," e.g. Millet et al. (2006)), a time-dependent quantity that describes the total amount of HCHO produced over multiple generations of oxidation. The total yield is typically derived from model simulations and used to relate satellite HCHO column observations to isoprene emissions (Marais et al., 2012; Millet et al., 2006). Early studies acknowledged the NO_x dependence of the total yield (Millet et al., 2006; Palmer et al., 2003), and more recent work has attempted to account for this dependence using NO_2 column observations (Marais et al., 2012). Here, we define the "prompt yield" as the change in observed HCHO per unit change in $ISOP_0$ ($\Delta HCHO/\Delta ISOP_0$). This is not the same as the first-generation yield, since the prompt yield can include HCHO production and loss over several hours (depending on the photochemical exposure of an air mass). Nor is it the same as the total yield, which inherently does not account for HCHO loss as an air mass ages. The prompt yield is effectively a quantity that relates isoprene emission strength to observed HCHO abundance. As we will demonstrate, this quantity is well-suited for segregating the various drivers of HCHO and for benchmarking model performance.

Figure 3A shows the relationship between calculated $ISOP_0$ and observed HCHO. The overall correlation is linear with a striking NO_x gradient. To quantify this NO_x dependence, we sort the data by $\log(NO_x)$, group it into 20 bins such that each bin contains the same number of points (N = 416), and perform a major-axis linear fit of HCHO versus $ISOP_0$ for each bin. Individual fits give r^2 values of 0.6-0.8, except for the highest NO_x bin (r^2 = 0.48) that contains some heavily-polluted air masses, such as downwind from power plants. Very fresh power plant plumes, defined as $\log(NO_x)$ values exceeding a mean + 3σ threshold, are removed prior to this procedure to avoid skewing the highest NO_x bin. Results are independent of the number of bins chosen or time resolution (e.g., 1-second versus 1-minute data).

The HCHO-$ISOP_0$ slope (Fig. 3B) represents the prompt yield. This yield varies by a factor of 3 over the range of observed NO_x, from 0.3 ppbv $ppbv^{-1}$ for NO_x mixing ratios of a few hundred pptv to 0.9 ppbv $ppbv^{-1}$ at NO_x > 1 ppbv. At low NO_x, the prompt yield is comparable to the MCM-predicted direct first-generation yield of HCHO (0.25-0.4 ppbv $ppbv^{-1}$ at NO = 10-40 pptv, Fig. S3), while at high NO_x it is somewhat higher than the predicted first-generation yield (0.75 ppbv $ppbv^{-1}$ at NO = 1000 pptv). This likely reflects the inclusion of more than one generation of HCHO production at higher NO_x, where oxidation is more rapid (median exposures increase by 38% over the range of observed NO_x values). Most of this portion of the HCHO budget, however, stems from first-generation production.

The intercept (Fig. 3C) represents the abundance of "background" HCHO. This portion of the HCHO budget stems mainly from air that either has not encountered strong isoprene emissions or is so aged that most of the isoprene has reacted away and can no longer be linked to a specific source region. Some of this background may also stem from oxidation of long-lived primary emissions like methane or methanol. Box model calculations (Sect. 5) indicate average HCHO budget contributions of 0.3 ± 0.2 ppbv and 0.2 ± 0.1 ppbv from methane and methanol, respectively. Background HCHO also exhibits a marked NO_x dependence, increasing from 1.6 to 3.3 ppbv over the observed NO_x range. As with the prompt yield, we expect such behavior since NO_x regulates the fate of all organic peroxy radicals (see Sect. 6). Assuming a 1 km mixed layer depth (Wagner et al., 2015), the corresponding HCHO column density for this background is 4 – 8 x 10^{15} cm^{-2}. This is comparable to the background reported by previous investigations of satellite-derived HCHO columns (Barkley et al., 2013; Millet et al., 2006). None of these studies explicitly account for the NO_x dependence of the background, though it can represent a substantial fraction of the total HCHO column – maximum summertime HCHO columns over the southeast U.S. are ~25 x 10^{15} cm^{-2} (Millet et al., 2008). Given the strong NO_x dependence of both prompt and background HCHO, grouping HCHO column observations by NO_x (e.g. using simultaneous observations of NO_2 columns (Marais et al., 2012) or model-derived NO_x) and performing an analysis similar to that described here could provide a robust means of accounting for these influences.

5 Model Evaluation

Next, we compare the observed HCHO-$ISOP_0$ relationship to results from a global chemical-transport model and a 0-D box model. Our goals are to both illustrate the utility of this analysis and evaluate model performance. By going beyond a simple comparison of modeled and measured mixing ratios, we can more accurately pinpoint potential shortcomings in model chemistry.

The GFDL AM3 model is an atmospheric general circulation model with interactive chemistry (Donner et al., 2011), including recent updates to the representation of isoprene degradation (Mao et al., 2013; Naik et al., 2013). Model simulations were carried out at 50 × 50 km^2 resolution with horizontal winds nudged to NCEP GFS analyses and sampled along the SENEX flight tracks at a time resolution of 1 minute. Further details are available elsewhere (Li et al., 2016).

The University of Washington Chemical Box Model (UWCM v2.2) is a versatile 0-dimensional framework for simulating various chemical systems, including lab chamber experiments (Wolfe et al., 2012) and observations from ground (Kim et al., 2015; Kim et al., 2013; Wolfe et al., 2014) and airborne (Marvin et al., 2015) platforms. Multiple chemical mechanisms are available within UWCM; here we used the latest version of the Master Chemical Mechanism (MCM v3.3.1, Jenkin et al. (2015)). UWCM was constrained with 1-minute average observations of isoprene, NO_2, ozone, CO, PAN, methane, methanol and meteorology and assumed clear-sky conditions for photolysis frequencies. The chemical system was integrated forward in time to diel steady state (total integration time of 3 days) for each set of measurements. This setup inherently assumes that the atmosphere is in chemical steady state – that is, that production and loss of HCHO, MVK, MACR and other species are roughly balanced. This assumption is rarely strictly true and may fail for highly-aged air masses (where isoprene is depleted) or when close to strong local emissions. Nonetheless, it is a fair approximation for the daytime well-mixed boundary layer observations that prevailed during SENEX. Monoterpenes and anthropogenic VOC are excluded from the simulation since observations of these species (from the iWAS) are relatively sparse. Separate sensitivity simulations utilizing the iWAS data suggest that observed monoterpenes and anthropogenic VOC (a subset of alkanes, alkenes and aromatics) increase modeled HCHO by 1 ± 2% and 2 ± 3%, respectively. A more detailed evaluation of box model performance is forthcoming (Marvin et al., 2015).

Output from both models is filtered for daytime, boundary-layer, non-biomass burning points using the same criteria as that for observations (Sect. 2). Both models adequately reproduce observed HCHO mixing ratios (Fig. S5). We perform the same analyses as described above to derive model prompt yield and background HCHO. Because of the reduced time resolution, we group results into 10 NO_x bins, instead of 20, before fitting. For AM3, this results in 172 points per bin and typical r^2 values of 0.4 – 0.8. For UWCM, there are 134 points per bin and all r^2 values are > 0.86.

Both AM3 and UWCM reproduce the observed NO_x dependence of the prompt yield (Fig. 4A). AM3 agrees well with observations in both magnitude and trend, though with some scatter at mid-NO_x levels. UWCM tends be slightly low throughout most of the NO_x range, which may reflect an issue with the mechanism (discussed below) or an inherent shortcoming of the steady-state assumption. Regardless of minor differences, these results suggest that both models provide excellent representation of early generation isoprene oxidation across NO_x regimes.

Background HCHO mixing ratios are under-predicted by 0.5 – 1 ppbv by both models (Fig. 4B). The range of under-prediction is consistent with the offsets between observed and modeled total HCHO abundances (Fig. S5 fit x-intercepts: 0.3 ppbv (AM3) and 1.1 ppbv (UWCM)). It is possible that both models are missing some HCHO precursors (e.g. from multi-generation isoprene oxidation or other VOC not related to isoprene). This is especially plausible for the UWCM simulation, which only includes isoprene, methane and methanol as primary VOC and does not account for horizontal transport. Under-estimated OH concentrations might also explain part of this discrepancy, though we cannot easily evaluate this possibility. AM3 performs somewhat better than UWCM in terms of overall magnitude but exhibits a less clear NO_x trend, which may reflect dilution over fairly large grid scales (note that the range of binned NO_x values is smaller for AM3 than both observations and the UWCM). This result again highlights the need to consider this background before using a model to interpret observed HCHO columns that effectively average HCHO sources over space and time.

The agreement between AM3 and UWCM-MCMv3.3.1 is consistent with how these mechanisms treat first-generation $ISOPO_2$ radicals (Figs. S6 and S7). Both models use the same rate constants for reactions of $ISOPO_2$ with NO and HO_2, which comprise the bulk of $ISOPO_2$ sink. The AM3 mechanism assigns a 12% yield of HCHO to the reaction of $ISOPO_2$

with HO_2 (Paulot et al., 2009b), while the MCM assumes 100% production of peroxides for this channel. This may explain some of the discrepancy in the prompt yield at low NO_x (Fig. 4A), though neither mechanism is consistent with the current experimental HCHO yield of ~6% HCHO (Liu et al., 2013). There are also two key differences in the minor reaction channels. First, the rate constant for reaction of $ISOPO_2$ with other RO_2 is an order of magnitude lower in AM3 compared to MCMv3.3.1 (1.54 vs. $12 – 16 \times 10^{-13}$ cm^3 s^{-1}, the latter depending on the $ISOPO_2$ isomer distribution). This reaction produces HCHO with yields comparable to that of $ISOPO_2$ + NO and may be an important source in very-low NO_x regimes. Second, AM3 assumes a constant $ISOPO_2$ isomer distribution and thus under-predicts the isomerization rate relative to MCMv3.3.1, especially at mid to high NO_x (Fig. S7D). AM3 also includes HCHO and other small oxidized VOC as direct products of isomerization rather than producing hydroperoxyaldehydes and other large products, which influences the timescale of HCHO production and thus the partitioning between prompt and background HCHO. The impact of the RO_2 reaction and isomerization channels on HCHO yields is likely minor but depends significantly on the RO_2/HO_2 ratio (at low NO_x) and on the overall $ISOPO_2$ lifetime, which affects the $ISOPO_2$ isomer distribution. For the particular model conditions in Fig. S3B, $ISOPO_2$ lifetimes for the two mechanisms can differ by as much as 25% at the lowest NO_x values (Fig. S7E). Regardless of these differences, the results shown in Fig. 4 confirm that both the condensed AM3 and explicit MCMv3.3.1 mechanisms perform similarly with regard to overall HCHO production.

6 Mechanistic Drivers of the NO_x – HCHO Relationship

Despite the complexity of gas-phase organic chemistry, the impact of NO_x on HCHO production essentially reduces to two factors: radical cycling and RO_2 branching. Increasing NO enhances the conversion of HO_2 to OH (R4) and thus accelerates VOC oxidation (R5). RO_2 is also produced, to a lesser extent, by VOC ozonolysis and photolysis (R6). Subsequent production of HCHO depends on the structure and fate of RO_2 intermediates, which can react with NO, HO_2, other RO_2, or isomerize (R7).

$$NO + HO_2 \rightarrow NO_2 + OH \quad \text{(R4)}$$

$$VOC + OH \rightarrow RO_2 \quad \text{(R5)}$$

$$VOC + (O_3/h\nu) \rightarrow RO_2 \quad \text{(R6)}$$

RO_2 + (NO, HO_2, RO_2, isomerization) → αHCHO (R7)

Here, α represents a bulk branching ratio for HCHO production weighted over all RO_2 reactions. The RO_2 lifetime is typically less than 100 s during the day, so (R5) is the rate-limiting step in HCHO formation. The HCHO production rate is then equal to the product of the total RO_2 production rate and the bulk branching ratio:

$$P(HCHO) = \alpha P(RO_2) \quad (3)$$

Though total RO_2 losses include reactions that do not make HCHO, α is still a useful metric for the relationship between HCHO production and overall VOC oxidation.

To disentangle these factors, we extract chemical rates from the diel steady-state UWCM simulations discussed in Sect. 5. Figure 5A shows the gross production rates for total peroxy radicals and HCHO as a function of NO_x. Consistent with our earlier discussion, HCHO production increases by a factor of 3 from low to high NO_x. Total RO_2 production increases by a factor of 2 over this same range, driven primarily by increasing OH. The bulk branching ratio α, calculated as the ratio of HCHO and RO_2 production rates, increases from 0.43 to 0.62 (Fig. 5B). This trend is consistent with NO_x-dependent branching ratios of several major HCHO precursors, including isoprene hydroxyperoxy radicals ($ISOPO_2$) and methyl peroxy radical (Fig. 5B). Based on this analysis, we conclude that enhanced OH production is the main driver for the NO_x dependence of HCHO production, with variations in RO_2 branching playing a lesser (but still important) role.

Using a combination of regional modeling and satellite observations, a recent study by Valin et al. (2016) also examines the drivers of HCHO production. They concur that OH production exerts a controlling influence on HCHO throughout the Southeast U.S. In contrast to our study, however, they assert that changes in RO_2 branching have a negligible effect on the HCHO-NO_x dependence. There are several potential explanations for this discrepancy. First, Valin et al. (2016) derive an "effective branching ratio" that is analogous to the bulk branching ratio in Eqn. (3) but calculated with reference to production of OH rather than RO_2. Many OH sinks do not form RO_2 radicals (e.g. reaction with CO, HCHO, methanol and NO_2) and thus will not make HCHO. The fractional contribution of such reactants to total modeled OH reactivity increases from 36% to 60% over our NO_x range; thus, using P(OH) instead of $P(RO_2)$ to calculate α from Eqn. (3) would effectively normalize out the NO_x dependence of RO_2 branching (Fig. 5B). Second, these two studies use very different photochemical

mechanisms. Valin et al. (2016) use a modified version of the lumped Regional Atmospheric Chemistry Mechanism 2 (RACM2) (Browne et al., 2014; Goliff et al., 2013), while our box model uses the explicit MCMv3.3.1 (Jenkin et al., 2015). In Valin et al. (2016), it is stated that increasing HCHO production from the RO_2 + RO_2 channel compensates for decreasing production from RO_2 + NO – an effect that we do not observe. Deeper investigation reveals that the rate constant for reaction of $ISOPO_2$ with HO_2 in RACM2 is a factor of 2 lower than those used in both MCMv3.3.1 and the AM3 mechanism, which are based on the experimentally-derived parameterization of Boyd et al. (2003). Thus, our model predicts a significantly larger contribution of RO_2 + HO_2 (which produces negligible HCHO) to the total RO_2 sink. These differences highlight the importance of carefully evaluating chemical mechanisms before using models to interpret *in situ* and satellite observations.

Increased OH also reduces the lifetime of HCHO, which may affect the HCHO budget if this reaction becomes competitive with photolysis. UWCM predicts an average HCHO photolysis lifetime of 4 hours and OH reaction lifetimes that range from 3 hours at high NO_x to 12 hours at low NO_x. Thus, photolysis is typically the dominant loss process and the scaling of HCHO lifetime with OH is typically weak. The net chemical tendency of HCHO (production minus loss) is positive and increasing throughout the range of model NO_x conditions. Faster loss due to reaction with OH therefore only slightly dampens the enhancement in HCHO production.

7 Conclusions

Using SENEX aircraft observations, we have quantified the NO_x dependence of the relationship between isoprene emission strength and HCHO mixing ratios. Simultaneous measurements of isoprene, MVK and MACR define a photochemical clock for isoprene oxidation, allowing separation of prompt HCHO production (which retains the isoprene source signature) and background HCHO from late-generation isoprene oxidation products, methane and other long-lived VOC. The prompt HCHO yield increases by a factor of 3 (0.3 to 0.9 ppbv $ppbv^{-1}$) and the average background HCHO mixing ratio doubles (1.6 to 3.3 ppbv) over the range of NO_x values encountered in the southeast U.S. (0.1 – 2 ppbv). This analytical method is applied to evaluate the performance of a global chemical transport model and a 0-D steady-state box model. Both models accurately reproduce the observed NO_x trend of the prompt HCHO yield, indicating that both chemical mechanisms accurately capture early-stage

isoprene oxidation. On the other hand, both models also under-predict background HCHO abundance by 0.5 – 1 ppbv, which is a significant fraction of total HCHO in some cases. This suggests insufficient build-up of isoprene-derived long-lived precursors in the models, missing VOC not related to isoprene, or insufficient OH. Box model results also provide insight into the mechanistic drivers of the observed NO_x trends. Over the NO_x range studied here, a 100% increase in total RO_2 production and a 40% increase in the HCHO production branching ratio give rise to a 3-fold increase in total HCHO production.

To our knowledge, there are no direct laboratory measurements of HCHO yields from low-NO_x isoprene chemistry; thus, the results presented here constitute the first measurement-constrained evaluation of the isoprene-HCHO link across NO_x regimes. The AM3 and MCMv3.3.1 mechanisms differ substantially (the former is highly condensed while the latter is explicit), but both contain recent updates to isoprene degradation. We expect that other mechanisms will also perform well if they accurately reflect our current best understanding. The observations presented here do not include the extremely-low NO_x regime (NO_x < 0.1 ppbv) typical of remote regions like the Amazon and equatorial Africa. In such pristine regions, smearing of HCHO production is expected to be more severe (Barkley et al., 2013), and total HCHO production may be significantly lower if the RO_2 fate favors functionalization over fragmentation (e.g. isomerization). More work is needed to map out this area of the urban-rural spectrum. It may also be possible to apply the methods developed here to evaluate the chemistry of glyoxal, another key tracer of VOC oxidation that is also amenable to orbital observations (Kaiser et al., 2015b; Li et al., 2016) and is believed to be an important precursor for SOA (McNeill et al., 2012).

These results also carry implications for top-down isoprene emission estimates. Uncertainties in low-NO_x chemistry are often cited as the largest source of potential error in derived emissions (Marais et al., 2012; Palmer et al., 2006). Based on our analysis, current mechanisms appear to capture low-NO_x production of HCHO, MVK and MACR, thus such errors are likely less severe than commonly asserted. Recent work has acknowledged the impact of NO_x on the prompt yield of HCHO from isoprene (Marais et al., 2012). We advocate considering the NO_x dependence of background HCHO as well, since this can constitute a significant fraction of the total HCHO column. For scale, the derived background HCHO mixing ratio of 1.6 – 3.3 ppbv is 37 – 77% of the campaign-mean observed HCHO mixing ratio of 4.3 ppbv. Forthcoming geostationary observations will resolve local gradients

in chemical regime, and smearing and background HCHO production will become problematic even in high-NO_x regions. Indeed, even current-generation orbital instruments are capable of resolving some urban-rural gradients in HCHO columns (Boeke et al., 2011). When applying advanced statistical techniques like inversion, model results will only be as accurate as the chemical mechanisms driving them. Continued field observations are crucial for providing confidence in our ability to link HCHO to its sources. In this regard, recent work has highlighted the potential of airborne eddy covariance fluxes to quantify both surface-atmosphere exchange and *in situ* chemical processes (Karl et al., 2013; Kaser et al., 2015; Misztal et al., 2014; Wolfe et al., 2015). With such tools, it should be possible to simultaneously measure both isoprene emissions and HCHO columns, thereby obtaining a direct experimental constraint on the link between these two quantities.

Data Availability

All data used in this study are publicly accessible on the SENEX website (http://www.esrl.noaa.gov/csd/projects/senex/).

Acknowledgements

We are grateful to NOAA AOC and the flight crew of the WP-3D for enabling a super awesome mission. HCHO measurement efforts were supported by US EPA Science to Achieve Results (STAR) program grant 83540601 and NASA grant NNH10ZDA001N-SEAC4RS. Analysis was supported by NASA ACCDAM grant NNX14AP48G. J. Kaiser acknowledges support from NASA ESSF grant NNX14AK97H. C.D. Hatch was supported by the Hendrix faculty grant and the Hendrix College Odyssey program. JM and LWH acknowledge support from NOAA Climate Program Office grant # NA13OAR4310071. This research has not been subjected to any EPA review and therefore does not necessarily reflect the views of the agency, and no official endorsement should be inferred.

References

Abbot, D. S., Palmer, P. I., Martin, R. V., Chance, K. V., Jacob, D. J., and Guenther, A.: Seasonal and interannual variability of North American isoprene emissions as determined by formaldehyde column measurements from space, Geophys. Res. Lett., 30, 1886, doi: 10.1029/2003GL017336, 2003.

Atkinson, R. and Arey, J.: Gas-phase tropospheric chemistry of biogenic volatile organic compounds: a review, Atmos. Env., 37, S197 - S219, 2003.

Atkinson, R., Baulch, D., Cox, R., Crowley, J., Hampson, R., Hynes, R., Jenkin, M., Rossi, M., and Troe, J.: Evaluated kinetic and photochemical data for atmospheric chemistry: Volume II - gas phase reactions of organic species, Atmos. Chem. Phys., 6, 3625-4055, 2006.

Barkley, M. P., De Smedt, I., Van Roozendael, M., Kurosu, T. P., Chance, K., Arneth, A., Hagberg, D., Guenther, A., Paulot, F., Marais, E., and Mao, J. Q.: Top-down isoprene emissions over tropical South America inferred from SCIAMACHY and OMI formaldehyde columns, J. Geophys. Res. Atmos., 118, 6849-6868, doi: 10.1002/jgrd.50552, 2013.

Barkley, M. P., Palmer, P. I., Kuhn, U., Kesselmeier, J., Chance, K., Kurosu, T. P., Martin, R. V., Helmig, D., and Guenther, A.: Net ecosystem fluxes of isoprene over tropical South America inferred from Global Ozone Monitoring Experiment (GOME) observations of HCHO columns, J. Geophys. Res., 113, D20304, doi: 10.1029/2008JD009863, 2008.

Boeke, N. L., Marshall, J. D., Alvarez, S., Chance, K. V., Fried, A., Kurosu, T. P., Rappengluck, B., Richter, D., Walega, J., Weibring, P., and Millet, D. B.: Formaldehyde columns from the Ozone Monitoring Instrument: Urban versus background levels and evaluation using aircraft data and a global model, J. Geophys. Res. Atmos., 116, D05303, doi: 10.1029/2010jd014870, 2011.

Boyd, A. A., Flaud, P. M., Daugey, N., and Lesclaux, R.: Rate Constants for RO2 + HO2 Reactions Measured under a Large Excess of HO2, J. Phys. Chem. A, 107, 818-821, 2003.

Brown, S. S., deGouw, J. A., Warneke, C., Ryerson, T. B., Dube, W. P., Atlas, E., Weber, R. J., Peltier, R. E., Neuman, J. A., Roberts, J. M., Swanson, A., Flocke, F., McKeen, S. A., Brioude, J., Sommariva, R., Trainer, M., Fehsenfeld, F. C., and Ravishankara, A. R.:

Nocturnal isoprene oxidation over the Northeast United States in summer and its impact on reactive nitrogen partitioning and secondary organic aerosol, Atmos. Chem. Phys., 9, 3027-3042, 2009.

Browne, E. C., Wooldridge, P. J., Min, K. E., and Cohen, R. C.: On the role of monoterpene chemistry in the remote continental boundary layer, Atmos. Chem. Phys., 14, 1225-1238, doi: 10.5194/acp-14-1225-2014, 2014.

Carlton, A. and Baker, K.: Photochemical Modeling of the Ozark Isoprene Volcano: MEGAN, BEIS, and Their Impacts on Air Quality Predictions, Env. Sci. Technol., 45, 4438-4445, doi: 10.1021/es200050x, 2011.

Cazorla, M., Wolfe, G. M., Bailey, S. A., Swanson, A. K., Arkinson, H. L., and Hanisco, T. F.: A new airborne laser-induced fluorescence instrument for in situ detection of Formaldehyde throughout the troposphere and lower stratosphere, Atmos. Meas. Tech., 8, 541-552, doi: 10.5194/amt-8-541-2015, 2015.

Crounse, J. D., Knap, H. C., Ørnsø, K. B., Jørgensen, S., Paulot, F., Kjaergaard, H. G., and Wennberg, P. O.: On the atmospheric fate of methacrolein: 1. Peroxy radical isomerization following addition of OH and O2, J. Phys. Chem. A, 116, 5756-5762, doi: 10.1021/jp211560u, 2012.

Crounse, J. D., Paulot, F., Kjaergaard, H. G., and Wennberg, P. O.: Peroxy radical isomerization in the oxidation of isoprene, Phys. Chem. Chem. Phys., 13, 13607-13613, 2011.

Curci, G., Palmer, P. I., Kurosu, T. P., Chance, K., and Visconti, G.: Estimating European volatile organic compound emissions using satellite observations of formaldehyde from the Ozone Monitoring Instrument, Atmos. Chem. Phys., 10, 11501-11517, doi: 10.5194/acp-10-11501-2010, 2010.

da Silva, G., Graham, C., and Wang, Z. F.: Unimolecular beta-Hydroxyperoxy Radical Decomposition with OH Recycling in the Photochemical Oxidation of Isoprene, Env. Sci. Technol., 44, 250-256, 2010.

de Gouw, J. and Warneke, C.: Measurements of volatile organic compounds in the earths atmosphere using proton-transfer-reaction mass spectrometry, Mass Spec. Rev., 26, 223-257, doi: 10.1002/mas.20119, 2007.

de Gouw, J. A., McKeen, S. A., Aikin, K. C., Brock, C. A., Brown, S. S., Gilman, J. B., Graus, M., Hanisco, T., Holloway, J. S., Kaiser, J., Keutsch, F. N., Lerner, B. M., Liao, J., Markovic, M. Z., Middlebrook, A. M., Min, K. E., Neuman, J. A., Nowak, J. B., Peischl, J., Pollack, I. B., Roberts, J. M., Ryerson, T. B., Trainer, M., Veres, P. R., Warneke, C., Welti, A., and Wolfe, G. M.: Airborne Measurements of the Atmospheric Emissions from a Fuel Ethanol Refinery, J. Geophys. Res. Atmos., 120, 4385-4397, doi: 10.1002/2015jd023138, 2015.

de Gouw, J. A., Middlebrook, A. M., Warneke, C., Goldan, P. D., Kuster, W. C., Roberts, J. M., Fehsenfeld, F. C., Worsnop, D. R., Canagaratna, M. R., Pszenny, A. A. P., Keene, W. C., Marchewka, M., Bertman, S. B., and Bates, T. S.: Budget of organic carbon in a polluted atmosphere: Results from the New England Air Quality Study in 2002, J. Geophys. Res., 110, D16305, doi: 10.1029/2004jd005623, 2005.

DiGangi, J. P., Boyle, E. S., Karl, T., Harley, P., Turnipseed, A., Kim, S., Cantrell, C., Maudlin Iii, R. L., Zheng, W., Flocke, F., Hall, S. R., Ullmann, K., Nakashima, Y., Paul, J. B., Wolfe, G. M., Desai, A. R., Kajii, Y., Guenther, A., and Keutsch, F. N.: First direct measurements of formaldehyde flux via eddy covariance: implications for missing in-canopy formaldehyde sources, Atmos. Chem. Phys., 11, 10565-10578, doi: 10.5194/acp-11-10565-2011, 2011.

Donner, L. J., Wyman, B. L., Hemler, R. S., Horowitz, L. W., Ming, Y., Zhao, M., Golaz, J.-C., Ginoux, P., Lin, S. J., Schwarzkopf, M. D., Austin, J., Alaka, G., Cooke, W. F., Delworth, T. L., Freidenreich, S. M., Gordon, C. T., Griffies, S. M., Held, I. M., Hurlin, W. J., Klein, S. A., Knutson, T. R., Langenhorst, A. R., Lee, H.-C., Lin, Y., Magi, B. I., Malyshev, S. L., Milly, P. C. D., Naik, V., Nath, M. J., Pincus, R., Ploshay, J. J., Ramaswamy, V., Seman, C. J., Shevliakova, E., Sirutis, J. J., Stern, W. F., Stouffer, R. J., Wilson, R. J., Winton, M., Wittenberg, A. T., and Zeng, F.: The Dynamical Core, Physical Parameterizations, and Basic Simulation Characteristics of the Atmospheric Component AM3 of the GFDL Global Coupled Model CM3, J.Climate, 24, 3484-3519, doi: 10.1175/2011jcli3955.1, 2011.

Dufour, G., Wittrock, F., Camredon, M., Beekmann, M., Richter, A., Aumont, B., and Burrows, J. P.: SCIAMACHY formaldehyde observations: constraint for isoprene emission estimates over Europe?, Atmos. Chem. Phys., 9, 1647-1664, 2009.

Fares, S., Paoletti, E., Loreto, F., and Brilli, F.: Bidirectional Flux of Methyl Vinyl Ketone and Methacrolein in Trees with Different Isoprenoid Emission under Realistic Ambient Concentrations, Environ Sci Technol, 49, 7735-7742, doi: 10.1021/acs.est.5b00673, 2015.

Fortems-Cheiney, A., Chevallier, F., Pison, I., Bousquet, P., Saunois, M., Szopa, S., Cressot, C., Kurosu, T. P., Chance, K., and Fried, A.: The formaldehyde budget as seen by a global-scale multi-constraint and multi-species inversion system, Atmos. Chem. Phys., 12, 6699-6721, doi: 10.5194/acp-12-6699-2012, 2012.

Fu, T. M., Jacob, D. J., Palmer, P. I., Chance, K., Wang, Y. X. X., Barletta, B., Blake, D. R., Stanton, J. C., and Pilling, M. J.: Space-based formaldehyde measurements as constraints on volatile organic compound emissions in east and south Asia and implications for ozone, J. Geophys. Res. Atmos., 112, D06312, doi: 10.1029/2006jd007853, 2007.

Fuchs, H., Hofzumahaus, A., Rohrer, F., Bohn, B., Brauers, T., Dorn, H., Haseler, R., Holland, F., Kaminski, M., Li, X., Lu, K., Nehr, S., Tillmann, R., Wegener, R., and Wahner, A.: Experimental evidence for efficient hydroxyl radical regeneration in isoprene oxidation, Nature Geosci., 6, 1023-1026, doi: 10.1038/NGEO1964, 2013.

Goliff, W. S., Stockwell, W. R., and Lawson, C. V.: The regional atmospheric chemistry mechanism, version 2, Atmos. Env., 68, 174-185, doi: 10.1016/j.atmosenv.2012.11.038, 2013.

González Abad, G., Liu, X., Chance, K., Wang, H., Kurosu, T. P., and Suleiman, R.: Updated Smithsonian Astrophysical Observatory Ozone Monitoring Instrument (SAO OMI) formaldehyde retrieval, Atmos. Meas. Tech., 8, 19-32, doi: 10.5194/amt-8-19-2015, 2015.

Guenther, A. B., Jiang, X., Heald, C. L., Sakulyanontvittaya, T., Duhl, T., Emmons, L. K., and Wang, X.: The Model of Emissions of Gases and Aerosols from Nature version 2.1 (MEGAN2.1): an extended and updated framework for modeling biogenic emissions, Geosci. Mod. Dev., 5, 1471-1492, doi: 10.5194/gmd-5-1471-2012, 2012.

Hogrefe, C., Isukapalli, S. S., Tang, X. G., Georgopoulos, P. G., He, S., Zalewsky, E. E., Hao, W., Ku, J. Y., Key, T., and Sistla, G.: Impact of Biogenic Emission Uncertainties on the Simulated Response of Ozone and Fine Particulate Matter to Anthropogenic Emission Reductions, J. Air Waste Man. Assoc., 61, 92-108, doi: 10.3155/1047-3289.61.1.92, 2011.

Jenkin, M. E., Young, J. C., and Rickard, A. R.: The MCM v3.3.1 degradation scheme for isoprene, Atmos. Chem. Phys., 15, 11433-11459, doi: 10.5194/acp-15-11433-2015, 2015.

Kaiser, J., Wolfe, G. M., Bohn, B., Broch, S., Fuchs, H., Ganzeveld, L. N., Gomm, S., Haseler, R., Hofzumahaus, A., Holland, F., Jager, J., Li, X., Lohse, I., Lu, K., Prevot, A. S. H., Rohrer, F., Wegener, R., Wolf, R., Mentel, T. F., Kiendler-Scharr, A., Wahner, A., and Keutsch, F. N.: Evidence for an unidentified non-photochemical ground-level source of formaldehyde in the Po Valley with potential implications for ozone production, Atmos. Chem. Phys., 15, 1289-1298, doi: 10.5194/acp-15-1289-2015, 2015a.

Kaiser, J., Wolfe, G. M., Min, K. E., Brown, S. S., Miller, C. C., Jacob, D. J., deGouw, J. A., Graus, M., Hanisco, T. F., Holloway, J., Peischl, J., Pollack, I. B., Ryerson, T. B., Warneke, C., Washenfelder, R. A., and Keutsch, F. N.: Reassessing the ratio of glyoxal to formaldehyde as an indicator of hydrocarbon precursor speciation, Atmos. Chem. Phys., 15, 7571-7583, doi: 10.5194/acp-15-7571-2015, 2015b.

Karl, T., Harley, P., Emmons, L., Thornton, B., Guenther, A., Basu, C., Turnipseed, A., and Jardine, K.: Efficient Atmospheric Cleansing of Oxidized Organic Trace Gases by Vegetation, Science, 330, 816 - 819, doi: 10.1126/science.1192534, 2010.

Karl, T., Misztal, P., Jonsson, H., Shertz, S., Goldstein, A., and Guenther, A.: Airborne Flux Measurements of BVOCs above Californian Oak Forests: Experimental Investigation of Surface and Entrainment Fluxes, OH Densities, and Damkohler Numbers, J. Atmos. Sci., 70, 3277-3287, doi: 10.1175/JAS-D-13-054.1, 2013.

Kaser, L., Karl, T., Yuan, B., Mauldin III, R. L., Cantrell, C. A., Guenther, A. B., Patton, E. G., Weinheimer, A. J., Knote, C., Orlando, J., Emmons, L., Apel, E., Hornbrook, R., Shertz, S., Ullmann, K., Hall, S., Graus, M., de Gouw, J., Zhou, X., and Ye, C.: Chemistry-turbulence interactions and mesoscale variability influence the cleansing efficiency of the atmosphere, Geophys. Res. Lett., 42, 10894-10903, doi: 10.1002/2015GL066641, 2015.

Kefauver, S. C., Filella, I., and Peñuelas, J.: Remote sensing of atmospheric biogenic volatile organic compounds (BVOCs) via satellite-based formaldehyde vertical column assessments, Int. J. Remote Sens., 35, 7519-7542, doi: 10.1080/01431161.2014.968690, 2014.

Kim, S., Kim, S. Y., Lee, M., Shim, H., Wolfe, G. M., Guenther, A. B., He, A., Hong, Y., and Han, J.: Impact of isoprene and HONO chemistry on ozone and OVOC formation in a semirural South Korean forest, Atmos. Chem. Phys., 15, 4357-4371, doi: 10.5194/acp-15-4357-2015, 2015.

Kim, S., Wolfe, G. M., Mauldin, L., Cantrell, C., Guenther, A., Karl, T., Turnipseed, A., Greenberg, J., Hall, S. R., Ullmann, K., Apel, E., Hornbrook, R., Kajii, Y., Nakashima, Y., Keutsch, F. N., DiGangi, J. P., Henry, S. B., Kaser, L., Schnitzhofer, R., Graus, M., Hansel, A., Zheng, W., and Flocke, F. F.: Evaluation of HOx sources and cycling using measurement-constrained model calculations in a 2-methyl-3-butene-2-ol (MBO) and monoterpene (MT) dominated ecosystem, Atmos. Chem. Phys., 13, 2031-2044, doi: 10.5194/acp-13-2031-2013, 2013.

Knighton, W. B., Herndon, S. C., Franklin, J. F., Wood, E. C., Wormhoudt, J., Brooks, W., Fortner, E. C., and Allen, D. T.: Direct measurement of volatile organic compound emissions from industrial flares using real-time online techniques: Proton Transfer Reaction Mass Spectrometry and Tunable Infrared Laser Differential Absorption Spectroscopy, Industrial & Engineering Chemistry Research, 51, 12674-12684, doi: 10.1021/ie202695v, 2012.

Kwok, E. S. C., Aschmann, S. M., Arey, J., and Atkinson, R.: Product formation from the reaction of the NO3 radical with isoprene and rate constants for the reactions of methacrolein and methyl vinyl ketone with the NO3 radical, Int. J. Chem. Kin., 28, 925-934, 1996.

Lee, M., Heikes, B. G., Jacob, D. J., Sachse, G., and Anderson, B.: Hydrogen peroxide, organic hydroperoxide, and formaldehyde as primary pollutants from biomass burning, J. Geophys. Res. Atmos., 102, 1301-1309, doi: 10.1029/96jd01709, 1997.

Lerner, B. M., Gilman, J. B., Kuster, W. C., and de Gouw, J. A., et al.: An improved, automated whole-air sampler and VOC GC-MS analysis system, in preparation, 2016.

Li, J., Mao, J., Min, K. E., Washenfelder, R. A., Brown, S. S., Kaiser, J., Keutsch, F. N., Volkamer, R., Wolfe, G. M., Hanisco, T. F., Pollack, I. B., Ryerson, T. B., Graus, M.,

Gilman, J. B., Lerner, B. M., Warneke, C., de Gouw, J. A., Middlebrook, A. M., Liao, J., Welti, A., Henderson, B. H., Donner, L. J., Cooke, W. F., Paulot, F., and Horowitz, L. W.: Observational constraints on glyoxal production from isoprene oxidation and its contribution to organic aerosol over the Southeast United States, Geophys. Res. Lett., submitted, 2016.

Liu, Y. J., Herdlinger-Blatt, I., McKinney, K. A., and Martin, S. T.: Production of methyl vinyl ketone and methacrolein via the hydroperoxyl pathway of isoprene oxidation, Atmos. Chem. Phys., 13, 5715-5730, doi: 10.5194/acp-13-5715-2013, 2013.

Luecken, D. J., Hutzell, W. T., Strum, M. L., and Pouliot, G. A.: Regional sources of atmospheric formaldehyde and acetaldehyde, and implications for atmospheric modeling, Atmos. Env., 47, 477-490, doi: 10.1016/j.atmosenv.2011.10.005, 2012.

Mao, J., Horowitz, L. W., Naik, V., Fan, S., Liu, J., and Fiore, A. M.: Sensitivity of tropospheric oxidants to biomass burning emissions: implications for radiative forcing, Geophys. Res. Lett., 40, 1241-1246, doi: 10.1002/grl.50210, 2013.

Mao, J., Ren, X., Brune, W. H., Van Duin, D. M., Cohen, R. C., Park, J. H., Goldstein, A. H., Paulot, F., Beaver, M. R., Crounse, J. D., Wennberg, P. O., DiGangi, J. P., Henry, S. B., Keutsch, F. N., Park, C., Schade, G. W., Wolfe, G. M., and Thornton, J. A.: Insights into hydroxyl measurements and atmospheric oxidation in a California forest, Atmos. Chem. Phys., 12, 8009-8020, doi: 10.5194/acp-12-8009-2012, 2012.

Marais, E. A., Jacob, D. J., Kurosu, T. P., Chance, K., Murphy, J. G., Reeves, C., Mills, G., Casadio, S., Millet, D. B., Barkley, M. P., Paulot, F., and Mao, J.: Isoprene emissions in Africa inferred from OMI observations of formaldehyde columns, Atmos. Chem. Phys., 12, 6219-6235, doi: 10.5194/acp-12-6219-2012, 2012.

Marvin, M., Wolfe, G. M., and Salawitch, R., et al.: Evaluating mechanisms for isoprene oxidation using a constrained chemical box model and SENEX observations of formaldehyde, in preparation, 2015.

McNeill, V. F., Woo, J. L., Kim, D. D., Schwier, A. N., Wannell, N. J., Sumner, A. J., and Barakat, J. M.: Aqueous-Phase Secondary Organic Aerosol and Organosulfate Formation in Atmospheric Aerosols: A Modeling Study, Env. Sci. Technol., 46, 8075-8081, doi: 10.1021/es3002986, 2012.

Millet, D. B., Jacob, D. J., Boersma, K. F., Fu, T. M., Kurosu, T. P., Chance, K., Heald, C. L., and Guenther, A.: Spatial distribution of isoprene emissions from North America derived from formaldehyde column measurements by the OMI satellite sensor, J. Geophys. Res. Atmos., 113, D02307, doi: 10.1029/2007jd008950, 2008.

Millet, D. B., Jacob, D. J., Turquety, S., Hudman, R. C., Wu, S. L., Fried, A., Walega, J., Heikes, B. G., Blake, D. R., Singh, H. B., Anderson, B. E., and Clarke, A. D.: Formaldehyde distribution over North America: Implications for satellite retrievals of formaldehyde columns and isoprene emission, J. Geophys. Res. Atmos., 111, D24S02, doi: 10.1029/2005jd006853, 2006.

Misztal, P. K., Karl, T., Weber, R., Jonsson, H. H., Guenther, A. B., and Goldstein, A. H.: Airborne flux measurements of biogenic volatile organic compounds over California, Atmos. Chem. Phys., 14, 10631-10647, doi: 10.5194/acpd-14-10631-2014, 2014.

Naik, V., Horowitz, L. W., Fiore, A. M., Ginoux, P., Mao, J., Aghedo, A. M., and Levy, H., II: Impact of preindustrial to present-day changes in short-lived pollutant emissions on atmospheric composition and climate forcing, J. Geophys. Res. Atmos., 118, 8086-8110, doi: 10.1002/jgrd.50608, 2013.

Palmer, P. I., Abbot, D. S., Fu, T. M., Jacob, D. J., Chance, K., Kurosu, T. P., Guenther, A., Wiedinmyer, C., Stanton, J. C., Pilling, M. J., Pressley, S. N., Lamb, B., and Sumner, A. L.: Quantifying the seasonal and interannual variability of North American isoprene emissions using satellite observations of the formaldehyde column, J. Geophys. Res. Atmos., 111, D12315, doi: 10.1029/2005jd006689, 2006.

Palmer, P. I., Jacob, D. J., Fiore, A. M., Martin, R. V., Chance, K., and Kurosu, T. P.: Mapping isoprene emissions over North America using formaldehyde column observations from space, J. Geophys. Res. Atmos., 108, 4180, doi: 10.1029/2002jd002153, 2003.

Paulot, F., Crounse, J. D., Kjaergaard, H. G., Kroll, J. H., Seinfeld, J. H., and Wennberg, P. O.: Isoprene photooxidation: new insights into the production of acids and organic nitrates, Atmos. Chem. Phys., 9, 1479-1501, 2009a.

Paulot, F., Crounse, J. D., Kjaergaard, H. G., Kurten, A., St Clair, J. M., Seinfeld, J. H., and Wennberg, P. O.: Unexpected Epoxide Formation in the Gas-Phase Photooxidation of Isoprene, Science, 325, 730-733, doi: 10.1126/science.1172910, 2009b.

Peeters, J., Muller, J.-F., Stavrakou, T., and Nguyen, V. S.: Hydroxyl Radical Recycling in Isoprene Oxidation Driven by Hydrogen Bonding and Hydrogen Tunneling: The Upgraded LIM1 Mechanism, J. Phys. Chem. A, 118, 8625-8643, doi: 10.1021/jp5033146, 2014.

Peeters, J. and Müller, J. F.: HOx radical regeneration in isoprene oxidation via peroxy radical isomerisations. II: experimental evidence and global impact, Phys. Chem. Chem. Phys., 12, 14227-14235, doi: 10.1939/c0cp00811g, 2010.

Peeters, J., Nguyen, T. L., and Vereecken, L.: HOx radical regeneration in the oxidation of isoprene, Phys. Chem. Chem. Phys., 11, 5935-5939, doi: 10.1039/b908511d, 2009.

Peeters, J., Vandenberk, S., Piessens, E., and Pultau, V.: H-atom abstraction in reactions of cyclic polyalkenes with OH, Chemosphere, 38, 1189-1195, 1999.

Pollack, I., Lerner, B., and Ryerson, T.: Evaluation of ultraviolet light-emitting diodes for detection of atmospheric NO2 by photolysis - chemiluminescence, J. Atmos. Chem., 65, 111-125, doi: 10.1007/s10874-011-9184-3, 2010.

Rivera-Rios, J. C., Nguyen, T. B., Crounse, J. D., Jud, W., St Clair, J. M., Mikoviny, T., Gilman, J. B., Lerner, B. M., Kaiser, J. B., de Gouw, J., Wisthaler, A., Hansel, A., Wennberg, P. O., Seinfeld, J. H., and Keutsch, F. N.: Conversion of hydroperoxides to carbonyls in field and laboratory instrumentation: Observational bias in diagnosing pristine versus anthropogenically controlled atmospheric chemistry, Geophys. Res. Lett., 41, 8645-8651, doi: 10.1002/2014gl061919, 2014.

Roberts, J. M., Marchewka, M., Bertman, S. B., Goldan, P., Kuster, W., de Gouw, J., Warneke, C., Williams, E., Lerner, B., Murphy, P., Apel, E., and Fehsenfeld, F. C.: Analysis of the isoprene chemistry observed during the New England Air Quality Study (NEAQS) 2002 intensive experiment, J. Geophys. Res., 111, D23S12, doi: 10.1029/2006jd007570, 2006.

Ryerson, T., Huey, L., Knapp, K., Neuman, J., Parrish, D., Sueper, D., and Fehsenfeld, F.: Design and initial characterization of an inlet for gas-phase NOy measurements from aircraft, J. Geophys. Res. Atmos., 104, 5483-5492, doi: 10.1029/1998JD100087, 1999.

Shim, C., Wang, Y., Choi, Y., Palmer, P. I., Abbot, D. S., and Chance, K.: Constraining global isoprene emissions with Global Ozone Monitoring Experiment (GOME) formaldehyde column measurements, J. Geophys. Res., 110, D24301, doi: 10.1029/2004jd005629, 2005.

St. Clair, J. M., Wolfe, G. M., Rivera-Rios, J. C., Crounse, J. D., Praske, E., Kim, M. J., Thayer, M. P., Skog, K. M., Keutsch, F. N., Wennberg, P. O., and Hanisco, T. F.: Investigation of a potential HCHO measurement artifact from ISOPOOH, in preparation, 2016.

Stavrakou, T., Müller, J.-F., de Smedt, I., Van Roozendael, M., van der Werf, G. R., Giglio, L., and Guenther, A.: Evaluating the performance of pyrogenic and biogenic emission inventories against one decade of space-based formaldehyde columns, Atmos. Chem. Phys., 9, 1037-1060, 2009.

Stavrakou, T., Müller, J. F., Bauwens, M., De Smedt, I., Van Roozendael, M., Guenther, A., Wild, M., and Xia, X.: Isoprene emissions over Asia 1979-2012: impact of climate and land-use changes, Atmos. Chem. Phys., 14, 4587-4605, doi: 10.5194/acp-14-4587-2014, 2014.

Stroud, C., Roberts, J., Goldan, P., Kuster, W., Murphy, P., Williams, E., Hereid, D., Parrish, D., Sueper, D., Trainer, M., Fehsenfeld, F., Apel, E., Riemer, D., Wert, B., Henry, B., Fried, A., Martinez-Harder, M., Harder, H., Brune, W., Li, G., Xie, H., and Young, V.: Isoprene and its oxidation products, methacrolein and methylvinyl ketone, at an urban forested site during the 1999 Southern Oxidants Study, J. Geophys. Res. Atmos., 106, 8035-8046, doi: 10.1029/2000JD900628, 2001.

Trainer, M., Williams, E., Parrish, D., Buhr, M., Allwine, E., Westberg, H., Fehsenfeld, F., and Liu, S.: Models and observations of the impact of natural hydrocarbons on rural ozone, Nature, 329, 705-707, doi: 10.1038/329705a0, 1987.

Valin, L. C., Fiore, A. M., Chance, K., and González Abad, G.: The role of OH production in interpreting the variability of CH2O columns in the southeast U.S, J. Geophys. Res. Atmos., doi: 10.1002/2015JD024012, 2016.

Wagner, N. L., Brock, C. A., Angevine, W. M., Beyersdorf, A., Campuzano-Jost, P., Day, D., de Gouw, J. A., Diskin, G. S., Gordon, T. D., Graus, M. G., Holloway, J. S., Huey, G., Jimenez, J. L., Lack, D. A., Liao, J., Liu, X., Markovic, M. Z., Middlebrook, A. M., Mikoviny, T., Peischl, J., Perring, A. E., Richardson, M. S., Ryerson, T. B., Schwarz, J. P., Warneke, C., Welti, A., Wisthaler, A., Ziemba, L. D., and Murphy, D. M.: In situ vertical profiles of aerosol extinction, mass, and composition over the southeast United States during SENEX and SEAC4RS: observations of a modest aerosol enhancement aloft, Atmos. Chem. Phys., 15, 7085-7102, doi: 10.5194/acp-15-7085-2015, 2015.

Warneke, C., de Gouw, J. A., Del Negro, L., Brioude, J., McKeen, S., Stark, H., Kuster, W. C., Goldan, P. D., Trainer, M., Fehsenfeld, F. C., Wiedinmyer, C., Guenther, A. B., Hansel, A., Wisthaler, A., Atlas, E., Holloway, J. S., Ryerson, T. B., Peischl, J., Huey, L. G., and Hanks, A. T. C.: Biogenic emission measurement and inventories determination of biogenic emissions in the eastern United States and Texas and comparison with biogenic emission inventories, J. Geophys. Res. Atmos., 115, D00F18, doi: 10.1029/2009jd012445, 2010.

Warneke, C., Trainer, M., de Gouw, J. A., Parrish, D. D., Fahey, D. W., Ravishankara, A. R., Middlebrook, A. M., Brock, C. A., Roberts, J. M., Brown, S. S., Neuman, J. A., Lerner, B. M., Lack, D., Law, D., Huebler, G., Pollack, I., Sjostedt, S., Ryerson, T. B., Gilman, J. B., Liao, J., Holloway, J., Peischl, J., Nowak, J. B., Aikin, K., Min, K. E., Washenfelder, R. A., Graus, M. G., Richardson, M., Markovic, M. Z., Wagner, N. L., Welti, A., Veres, P. R., Edwards, P., Schwarz, J. P., Gordon, T., Dube, W. P., McKeen, S., Brioude, J., Ahmadov, R., Bougiatioti, A., Lin, J., Nenes, A., Wolfe, G. M., Hanisco, T. F., Lee, B. H., Lopez-Hilfiker, F. D., Thornton, J. A., Keutsch, F. N., Kaiser, J., Mao, J., and Hatch, C.: Instrumentation and Measurement Strategy for the NOAA SENEX Aircraft Campaign as Part of the Southeast Atmosphere Study 2013, Atmos. Meas. Tech. Discuss., 2016, 1-39, doi: 10.5194/amt-2015-388, 2016.

Wolfe, G. M., Cantrell, C., Kim, S., Mauldin III, R. L., Karl, T., Harley, P., Turnipseed, A., Zheng, W., Flocke, F., Apel, E. C., Hornbrook, R. S., Hall, S. R., Ullmann, K., Henrey, S. B., DiGangi, J. P., Boyle, E. S., Kaser, L., Schnitzhofer, R., Hansel, A., Graus, M., Nakashima, Y., Kajii, Y., Guenther, A., and Keutsch, F. N.: Missing peroxy radical sources within a summertime ponderosa pine forest, Atmos. Chem. Phys., 14, 4715-4732, doi: 10.5194/acp-14-4715-2014, 2014.

Wolfe, G. M., Crounse, J. D., Parrish, J. D., St. Clair, J. M., Beaver, M. R., Paulot, F., Yoon, T. P., Wennberg, P. O., and Keutsch, F. N.: Photolysis, OH reactivity and ozone reactivity of a proxy for isoprene-derived hydroperoxyenals (HPALDs), Phys. Chem. Chem. Phys., 14, 7276-7286, doi: 10.1039/c2cp40388a, 2012.

Wolfe, G. M., Hanisco, T. F., Arkinson, H. L., Bui, T. P., Crounse, J. D., Dean-Day, J., Goldstein, A., Guenther, A., Hall, S. R., Huey, G., Jacob, D. J., Karl, T., Kim, P. S., Liu, X., Marvin, M. R., Mikoviny, T., Misztal, P. K., Nguyen, T. B., Peischl, J., Pollack, I., Ryerson, T., St Clair, J. M., Teng, A., Travis, K. R., Ullmann, K., Wennberg, P. O., and Wisthaler, A.: Quantifying sources and sinks of reactive gases in the lower atmosphere using airborne flux observations, Geophys. Res. Lett., 42, 8231-8240, doi: 10.1002/2015GL065839, 2015.

Xu, L., Guo, H., Boyd, C. M., Klein, M., Bougiatioti, A., Cerully, K. M., Hite, J. R., Isaacman-VanWertz, G., Kreisberg, N. M., Knote, C., Olson, K., Koss, A., Goldstein, A. H., Hering, S. V., de Gouw, J., Baumann, K., Lee, S.-H., Nenes, A., Weber, R. J., and Ng, N. L.: Effects of anthropogenic emissions on aerosol formation from isoprene and monoterpenes in the southeastern United States, P. Nat. Acad. Sci. USA, 112, 37-42, doi: 10.1073/pnas.1417609112, 2015.

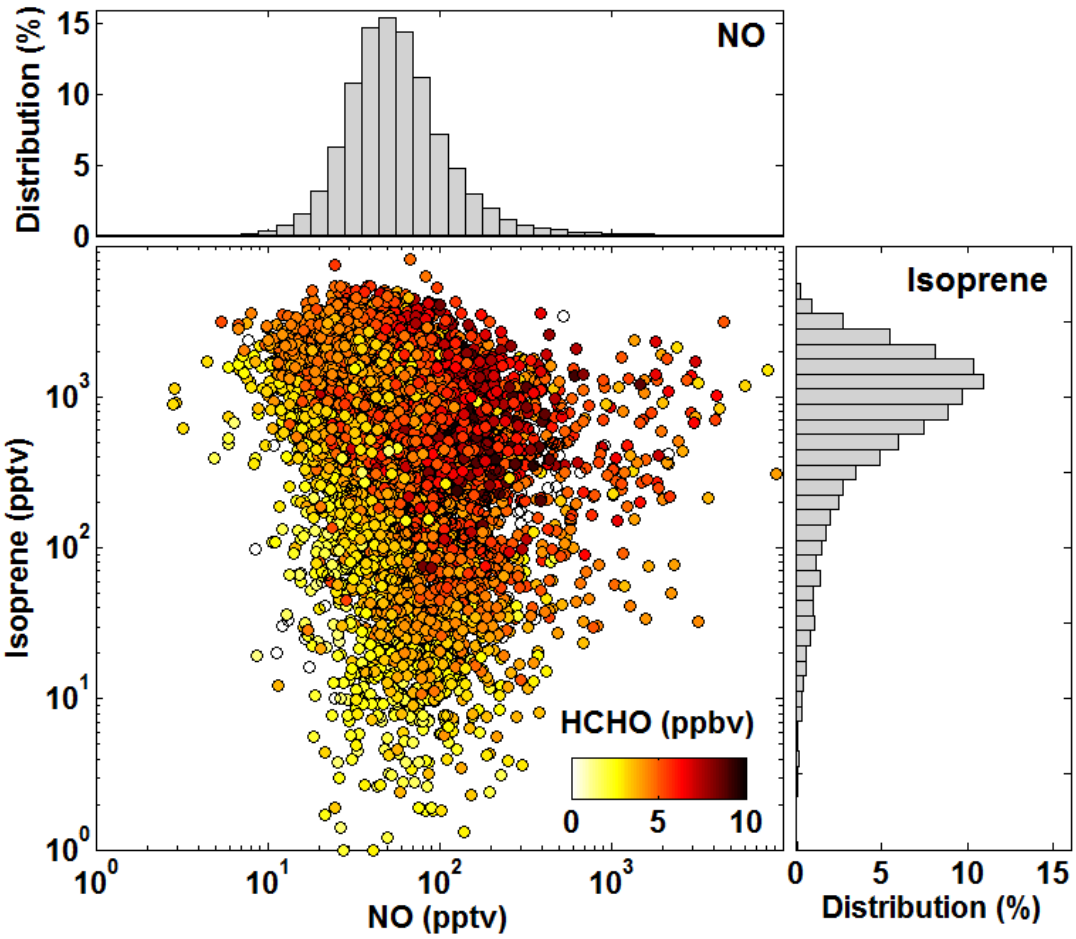

1

2

3 **Figure 1.** Co-variation of isoprene, NO and HCHO mixing ratios in the summertime
4 Southeast U.S. Data are limited to daytime boundary layer observations. Histograms show the
5 corresponding NO and isoprene distributions.

6

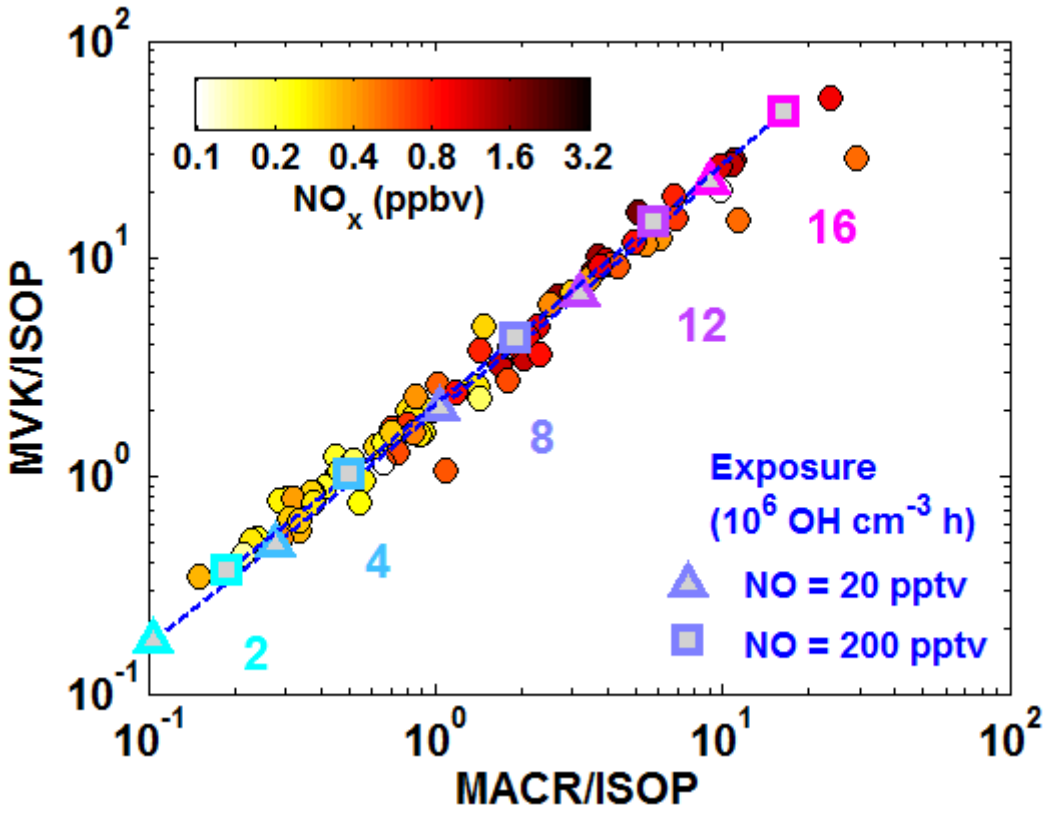

Figure 2. A photochemical clock of isoprene oxidation defined by the progression of daughter/parent ratios. Solid circles show the observed ratios calculated from iWAS observations, colored by NO_x. Blue/purple symbols, dashed lines, and text indicate the theoretical exposures (the product of OH concentration and time) corresponding to any given daughter/parent relationship. Theoretical values are calculated at 298K using MVK and MACR yields for NO values of 20 pptv (triangles) and 200 pptv (squares).

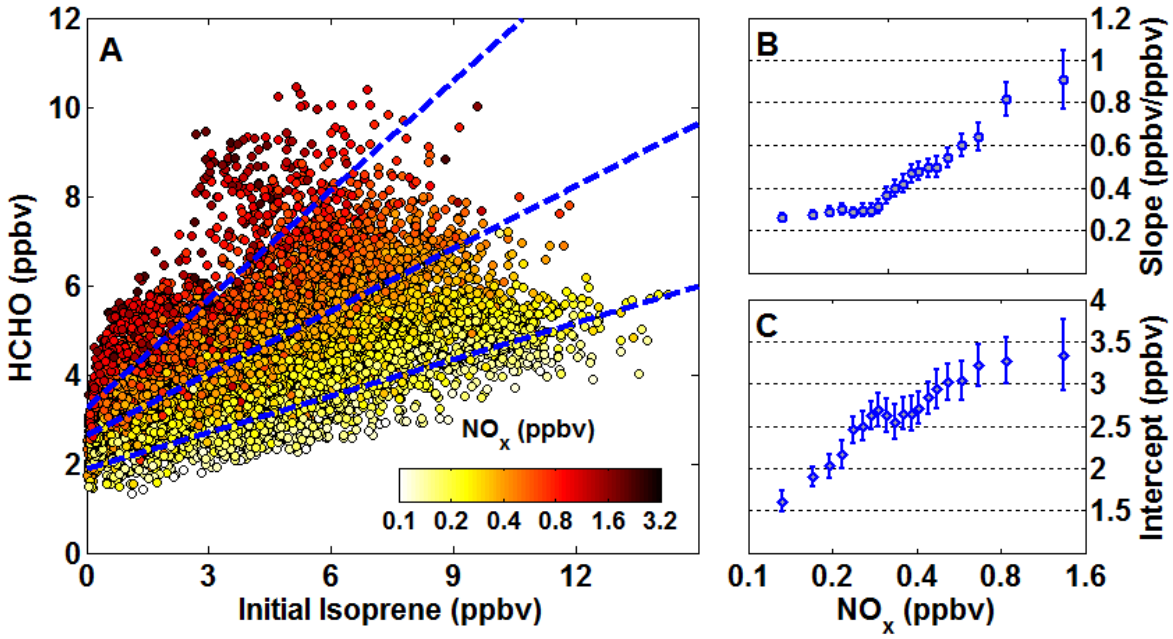

Figure 3. (A) NO_x modulates the relationship between observed HCHO and calculated initial isoprene mixing ratios. Symbols denote all 1-second data. Dashed lines illustrate representative major-axis fits of NO_x-grouped subsets at mean NO_x values of 170, 380 and 810 pptv (see text for details of fitting procedure). The slope (B) and intercept (C) of these fits are the prompt HCHO yield and background HCHO mixing ratio, respectively. Error bars in (B) and (C) are 3σ fitting uncertainties.

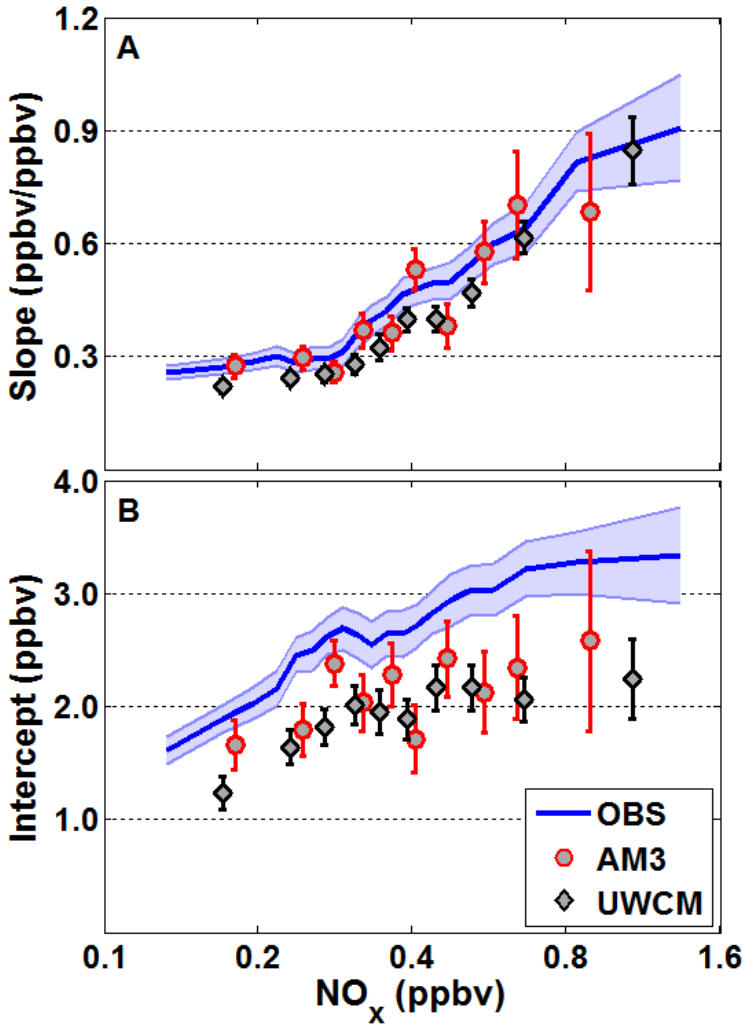

Figure 4. Comparison of observed and model-derived relationships between HCHO and initial isoprene versus NO_x. Slopes (A) and intercepts (B) are calculated as described in the text. The observed values (blue line with shading) are the same as those shown in Figs. 3B-C. Symbols represent fit results for the global AM3 model (red circles) and the 0-D UWCM box model (black diamonds). Error bars denote 3σ fitting uncertainties.

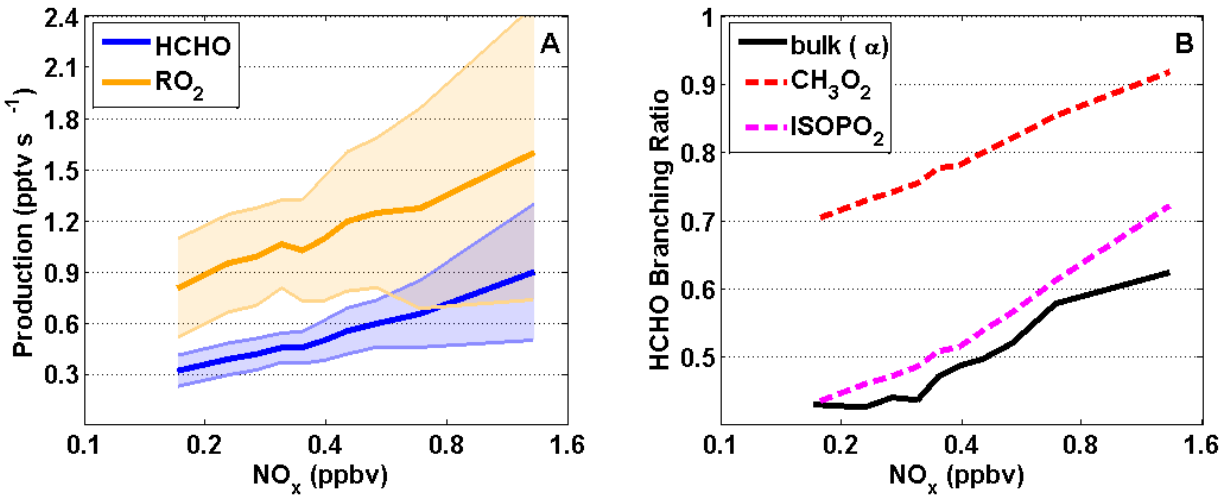

Figure 5. NO_x dependence of chemical properties related to HCHO production, extracted from the UWCM simulation of SENEX observations. (A) Production rates for HCHO (blue) and total RO_2 (orange). (B) Branching ratios for HCHO production weighted over all RO_2 (solid black line) and for several individual RO_2, including methyl peroxy radical (red) and total isoprene hydroxyperoxy radicals (magenta). All quantities are averaged over NO_x using 10 bins with equal numbers of points. In (A), solid lines show the mean and shading is 1σ variability.